Journal of the European Ceramic Society 32 (2012) 1269-1274.

Sintering and Dielectric Properties of Perovskite $SrTaO_2N$ Ceramics

Ya-Ru Zhang*, Teruki Motohashi**, Yuji Masubuchi and Shinichi Kikkawa

Graduate School of Engineering, Hokkaido University, N13W8, Kita-ku, Sapporo 060-8628, Japan

Single-phase perovskite oxynitride $SrTaO_2N$ ceramics were prepared by pressureless sintering at 1400 °C under a nitrogen atmosphere, using 5 wt% of $SrCO_3$ or La_2O_3 as a sintering additive. In contrast, $SrTaO_2N$ bulks without additives contained TaC and Ta_3N_5 impurities. Sintering in nitrogen led to oxygen/nitrogen deficiencies in the oxynitride, while post annealing in flowing ammonia was effective to eliminate the anion vacancies. The introduction of additives significantly improved the sinterability of $SrTaO_2N$ ceramics. A relative density of >90% in the bulk was achieved with a highly dense microstructure with smaller grain sizes. The $SrTaO_2N$ bulk with $SrCO_3$ additive exhibited superior dielectric performance with a high relative permittivity (ε_r = 1.0×10^4) and dissipation factor (tan δ = 0.039) at a frequency of 1 MHz.

Keywords: Perovskite oxynitrides; Sintering; Dielectric property; Sintering additives

*, ** Corresponding authors. E-mail addresses: yrzhang@eng.hokudai.ac.jp (Y.-R. Zhang), t-mot@eng.hokudai.ac.jp (T. Motohashi).

Introduction

High-permittivity dielectric materials play a significant role in microelectronics, due to their numerous technological applications such as capacitors and memory devices. To date, the most widely used dielectric ceramics are lead-based perovskite ferroelectrics or relaxor oxides, *e.g.*, $Pb(Zr,Ti)O_3$ (PZT) and $Pb(Mg_{1/3}Nb_{2/3})O_3$ (PMN) [1,2]. However, the toxicity of lead and its high vapor pressure during sintering have led to a demand for alternative environmentally friendly lead-free dielectric materials.

Recently, perovskite transition metal oxynitrides with the general formula of $AB(O,N)_3$ have drawn much attention due to their superior dielectric properties [3-7]. Within the oxynitride family, samples of the $SrTaO_2N$ ceramic were reported to possess large dielectric permittivity of ca. 2900 with moderate temperature dependence over the range of 180-300 K [3]. To date, the origin for this dielectric behavior has been studied on the basis of structural investigations [3,8,9]. It is suggested that the *cis* arrangement of nitrogen in TaO_4N_2 octahedra may induce tilting of each octahedron [9]. In $SrTaO_2N$ with statistically-averaged centrosymmetric *I*4/*mcm* space group, the coupling of anion ordering with octahedral tilting could lead to structural arrangements that possess a local dipole, which displays a similarity to the polar nanoregions (PNRs) in relaxor ferroelectrics [10]. Accordingly, the nonzero polar momentum units in $SrTaO_2N$ result in high dielectric permittivity under an applied electric field. $SrTaO_2N$ ceramics with large permittivity are stable in air, water and even in

concentrated acids.

One of the problems pertaining to dielectric oxynitride ceramics is the difficulty in fabricating high-density ceramics. There are only a few reports on dielectric oxynitrides [3-7], especially in the ceramic form [3]. The reported $SrTaO_2N$ bulks have considerable porosity (~45%) when sintered by means of a conventional method, which is far from ideal for assessment of the inherent dielectric properties, because these measurements are always affected by the grain interfaces. Therefore, the densification of $SrTaO_2N$ ceramics is necessary for fundamental characterization and also for practical applications, and should therefore be subject to further careful investigation. Hot pressing, hot isostatic pressing and spark plasma sintering are often used to achieve the densification of ceramics. However, these techniques are expensive when applied to mass production in commercial applications. Therefore, we have considered pressureless sintering with certain additives as a far more practical solution. The sintering of dielectric perovskite oxides can be promoted by the addition of A-site donor dopants because the densification kinetics is enhanced by the subsequently-induced A-site defects [11-13]. Meanwhile, during the sintering process of dielectric materials, incorporation of suitable additives could compensate the loss of easy-to-volatilize components. Yang *et al.* reported that the evaporation of PbO in PMN could be compensated by doping with SrO, resulting in the decrease of sintering temperature from 1200 to 800 ^{o}C as well as smaller grain sizes [14]. In addition, the dielectric properties can also be improved using specific dopants.

For instance, Kim *et al*. reported that the relative dielectric permittivity of La-modified $PbTiO_3$ with A-site vacancies was an order of magnitude larger than those of relaxor ferroelectrics [15]. Meanwhile, for PZT ceramics the isovalent substitution of Sr^{2+} for Pb^{2+} at the A-site led to a high dielectric constant of $1.0\text{-}1.3\times10^3$ due to the increased tetragonality [16]. Accordingly, $SrCO_3$ and La_2O_3 can be considered as potential sintering additives for the development of dense $SrTaO_2N$ bulks with high permittivity.

In the present work, the pressureless sintering, microstructure, and dielectric performance of $SrTaO_2N$ ceramics with and without additives was investigated. To the best of our knowledge, this is the first report on the sintering behavior of $SrTaO_2N$ with resulting high relative density.

Experimental Procedure

The perovskite oxynitride $SrTaO_2N$ was synthesized by ammonolysis of precursors obtained from a citrate route [17]. Stoichiometric amounts of $SrCO_3$ (Wako Pure Chemicals, 99.9%) and $TaCl_5$ (Sigma-Aldrich, 99.99%) powders were dissolved in 60 mL of anhydrous ethanol, in which citric acid (Wako Pure Chemicals, 98.0%) was added as a complexing agent. The amount of citric acid was equimolar to that of the Ta ions. The solution was heated and stirred at 150 °C to promote polymerization. The resultant viscous gel was then pre-fired at 350 °C for 1 h, which resulted in brownish amorphous oxide precursors. The ammonolysis

reaction was carried out in flowing ammonia (Sumitomo Seika Chemicals, 99.9%, 50 mL/min) at 1000 °C with a heating rate of 5 °C/min, then held for 12 h before cooling to room temperature.

The as-nitrided $SrTaO_2N$ powders were mixed with 5 wt% $SrCO_3$ or La_2O_3 (Sigma-Aldrich, 99.9%; fired at 970°C for 4 h prior to use) as an additive. Our preliminary experiments indicated that the sintered density and dielectric permittivity of $SrTaO_2N$ ceramics increased significantly when the additive amount was 5 wt% but further excessive addition had negative effects. These powders were die-pressed into 7 mm diameter and 2 mm thick disks, followed by cold isostatic pressing (CIP) at 150 MPa. $SrTaO_2N$ and $SrTaO_2N$ with $SrCO_3$ or La_2O_3 additive (hereafter denoted as $SrTaO_2N$-Sr and $SrTaO_2N$-La, respectively) were placed in a BN crucible and sintered at 1400 °C for 3 h under a nitrogen pressure of 0.2 MPa using a graphite furnace (High Multi 500; Fuji Dempa Kogyo). The sintered bulks were then annealed at 1000 °C for 12 h in flowing ammonia. This post-annealing procedure was necessary to obtain highly resistive bulks for reliable dielectric property measurements.

The $SrTaO_2N$ products were characterized using X-ray diffraction (XRD) with Cu *K*α radiation (Rigaku, Ultima IV). The data were collected over the angular range of 10-120° with a step size of 0.02°. A counting time of 2.0 s per step was used for the phase identification, while a longer counting time of 9.0 s per step was required for the structural refinement. The

lattice parameters of the $SrTaO_2N$ products, including as-nitrided powder, as-sintered and post-annealed bulks (in powder form), were refined by the Rietveld method using RIETAN2000 software [18]. The bulk density was measured by both the geometric and Archimedes methods. Scanning electron microscopy (SEM; Jeol JSM-6390LA) was used to observe the microstructure of the ceramics. The post-annealed samples were polished with a 4000-grit sandpaper (particle size: 3 μm) to obtain parallel surfaces and then coated with silver paste to act as electrodes. The dielectric properties were measured with impedance analyzers (Yokogawa-Hewlett-Packard, 4274A; Hewlett-Packard, 4285A) in the frequency range from 10^2 to 10^6 Hz at room temperature. The impedance plots were fitted and extrapolated using the Cole-Cole empirical relation [19].

Results and discussion

Figure 1 shows XRD patterns for the $SrTaO_2N$ powder, as-sintered $SrTaO_2N$ and post-annealed $SrTaO_2N$ bulks with and without sintering additives. Compared with the as-nitrided powder, a small amount of TaC impurity was detected in the as-sintered $SrTaO_2N$ bulk without any additive. The TaC impurity is likely to form when excess Ta is combined with organic residue due to the loss of SrO from $SrTaO_2N$ during sintering. To minimize the amount of organic residue in the precursor powder, the combustion at 600 °C was examined, but this procedure did not lead to a reduced amount of TaC in the as-sintered $SrTaO_2N$ bulk.

In spite of the high melting temperature, SrO loss may occur in high-temperature processing, as reported in $SrTiO_3$, $SrZrO_3$ and Sr_2RuO_4 [20-22]. The diffraction peaks of TaC impurity disappeared in the as-sintered $SrTaO_2N$-Sr and $SrTaO_2N$-La bulks because Sr^{2+} or La^{3+} from the additives compensates the Sr loss, which inhibits the appearance of this secondary phase. It was found that all the sintered bulks changed from brown to dark gray, which indicates reduction of the tantalum associated with anion deficiencies in the crystal lattice. Post-annealing in an ammonia atmosphere was necessary because heat treatment in air/oxygen leads to oxidation and decomposition of the oxynitrides [23]. After the annealing process, TaC and Ta_3N_5 impurities were observed in $SrTaO_2N$ without additives, while both $SrTaO_2N$-Sr/La samples were phase-pure perovskites. At high temperatures, the TaC impurity was oxidized and then nitrided in ammonia to form Ta_3N_5 in the post-annealed $SrTaO_2N$ bulk [24], as indicated in Fig. 1(e). We tentatively believe that a trace amount of oxygen from the not-fully airtight furnace is the oxidizing agent. It can be assumed that a part of TaC was not oxidized and still remained as it was, due to the limited amount of oxygen.

The XRD patterns were refined to obtain the lattice parameters of the $SrTaO_2N$ products, including the as-nitrided powder, as-sintered and post-annealed bulks, based on the tetragonal *I*4/*mcm* space group [9]. A summary of the crystallographic features is given in Table 1. Rietveld refinement plots for the $SrTaO_2N$ products are given in the Supporting Information. A trace amount (0.43 wt%) of $SrCl_2 \cdot 2H_2O$ impurity was observed in the as-nitrided powder.

The *c* parameter of the tetragonal lattice was slightly reduced in the as-sintered bulk. Recovery of the *c* value was then achieved by annealing in ammonia, which was accompanied by the color change from dark gray to brown. The lattice parameter variations upon sintering/post-annealing were reproducible in different sample batches. It is thus reasonable to interpret the lattice parameter variations as a hint for the changing anion vacancy contents upon sintering/post-annealing. Anion vacancies are assumed to be introduced during the high temperature sintering, because the thermal reduction environment in the graphite dies led to oxygen/nitrogen deficiency. However, the anion vacancies should be mainly ascribed to a loss of nitrogen because the reported standard free energy of formation is much lower for metal nitrides than for the corresponding oxides [25]. Compared with transition metal oxides, the relatively low stability of the associated nitrides, related to weaker bonding, has already been understood through theoretical calculations [26]. Therefore, the loss of nitrogen is more likely to occur by heating $SrTaO_2N$ at 1400 °C, which results in shrinking of the crystal lattice due to its covalent nature. The formation of nitrogen vacancies may involve the release of N_2 gas, as suggested by the previous thermogravimetric study [23]. Similar results have been documented in nonstoichiometric metal nitrides, such as TiN_x and δ-NbN_x [27].

The relative densities of the post-annealed $SrTaO_2N$, $SrTaO_2N$-Sr and $SrTaO_2N$-La bulks were 70, 93, and 90%, respectively. The $SrTaO_2N$ bulk without additives could not be well sintered, while a high density was achieved at 1400 °C by the addition of 5 wt% $SrCO_3$ or

La_2O_3. The fracture surface morphology did not change with the post-annealing, but was changed by the addition of sintering additives, as shown by the SEM micrographs in Fig. 2. After the annealing process, densification and smaller grain size was achieved with the sintering additives. The $SrTaO_2N$ bulk without additives was porous with large voids between the grains, indicating insufficient densification. In contrast, the $SrTaO_2N$ ceramics sintered with additives were considerably dense and consisted of a well-developed microstructure. The reason lies in that the SrO (from $SrCO_3$) or La_2O_3 could react with Sr-deficient $SrTaO_2N$ ($Sr_{1-\delta}TaO_2N$) to promote the efficient reaction sintering and further densification, while no obviously segregated compounds such as strontium tantalum oxides and lanthanum tantalum oxides were observed in the microstructures. Take the $SrTaO_2N$-La as an example, La^{3+} could partly substitute the A-site Sr^{2+}, due to their similar ionic radii [28]. The entropy gain by $(Sr_{1-x}La_x)Ta(O,N)_{3-\delta}$ solid solution formation are beneficial to mass transport and enhancement of the densification process. The loss of SrO offered an opportunity for the reaction sintering after the incorporation of additives, which was found to be necessary to obtain relatively dense $SrTaO_2N$ bulks. It is noteworthy that smaller grains were obtained in the $SrTaO_2N$-Sr/La ceramics. As the densification occurs, Sr^{2+}/La^{3+} appears not only in the bulk regions but also near grain boundaries due to the relatively high additive level, resulting in the inhibition of grain growth as well as the smaller grain sizes [29-31].

All the as-sintered $SrTaO_2N$ ceramics exhibited semiconductive behavior, typically with

several thousand ohms at room temperature. The successive heat treatment in ammonia was found to be essential to recover the dielectric properties which accompany resistance values several order of magnitudes larger than those of the as-sintered bulks. Figure 3 shows the dielectric constant (ε_r) and dielectric loss ($\tan\delta$) as a function of frequency for the post-annealed $SrTaO_2N$ samples. Both the ε_r and $\tan\delta$ values decrease with increasing frequency. The $SrTaO_2N$ bulk samples without additives have ε_r values in the order of 1.8×10^3 at 10^2 Hz, which is lower than that reported previously [3], despite its relatively higher density. It seems that the presence of secondary phases such as TaC and Ta_3N_5 is responsible for the lower dielectric constant. In contrast, the addition of $SrCO_3$ or La_2O_3 resulted in a significant increase in the dielectric constant, which was enhanced to 1.6×10^4. This value is several times higher than the permittivity (~2900) reported by Kim *et al.* [3]. The permittivity of $SrTaO_2N$-Sr/La ceramics is comparable to those reported for ferroelectric and relaxor oxides at their Curie temperatures [32]. Another intriguing feature of $SrTaO_2N$ with additives is the weak dependence of the dielectric constant on frequency, *e.g.*, $SrTaO_2N$-Sr had high relative permittivities of 1.7×10^4, 1.3×10^4, and 1.0×10^4 at frequencies of 10^2, 10^4, and 10^6 Hz, respectively. The dielectric constants of the $SrTaO_2N$ ceramics are sensitive to density. Enhanced densification is beneficial to obtain desirable dielectric properties. Accordingly, the highly densified $SrTaO_2N$-Sr/La bulks with uniform grain structure also exhibit much higher room-temperature dielectric constants than $SrTaO_2N$ without additives.

It is worthy to note that the dielectric loss for the present $SrTaO_2N$ bulk without additives is comparable to that obtained for a $LaTiO_xN_y$ thin film [5], which is an order of magnitude lower than that reported for the $SrTaO_2N$ bulk in the previous work [3]. It has been indicated that the dielectric loss decreases significantly as the sample sintering improves, while the electrical conductivity remains low [3]. The present $SrTaO_2N$-Sr/La bulks has a significantly improved grain microstructure, but the dielectric loss is relatively high. The tan δ values are all approximately 0.04 at 1 MHz, which is still higher than that required for practical applications. The number of grain boundaries was increased in the $SrTaO_2N$-Sr/La bulks due to the smaller grain size, leading to an accumulation of the space charge [33]. This may be one reason for the high dissipation factor. In addition, the formation of lattice defects within the crystal also affects the dielectric loss. The $SrTaO_2N$ ceramics with additives are well densified; therefore, it is likely that the anion deficiencies were not completely removed during the post annealing process. A small amount of anion vacancies (or tetravalent tantalum) is sufficient to cause a large increase in the dielectric loss [34]. Such Ta^{4+} species with paramagnetic moments should be detectable by means of electron paramagnetic resonance and be subject to further exploration. A similar result was also reported for $BaTi_4O_9/Ba_2Ti_9O_{20}$-based ceramics, where even a low defect density caused by reductive heat treatment significantly increased the dielectric loss [35].

Complex impedance plots of the $SrTaO_2N$ and $SrTaO_2N$-Sr/La bulks are shown in Fig. 4.

To interpret these impedance spectra, an equivalent circuit model consisting of two parallel RC elements connected in series was assumed. These two serial RC units represent the bulk (R_b) and grain boundary (R_{gb}) contributions [3]. For the $SrTaO_2N$-Sr/La bulks, the first semicircle corresponding to the bulk contribution was clearly observed, whereas the low frequency ($<10^2$ Hz) semicircle related to the grain boundaries was not evident due to the instrumental limitations of the experimental range. It has been recognized that the choice of the electrical contact type sometimes influences the overall electrical behaviors [36]. Nevertheless, effects of the electrodes are assumed to be insignificant, since different contact types (here Ag-pasted and Pt-sputtered electrodes) resulted in essentially similar results, as presented in Supporting Information. The R_b value, assigned as the intercept of the Z'-axis in the Cole-Cole plot, is quite different among the $SrTaO_2N$ and $SrTaO_2N$-Sr/La bulks. The impedance spectrum of the $SrTaO_2N$ bulk without additives did not form a semicircle, which is indicative of a much higher value for R_b. The lower bulk resistance of the $SrTaO_2N$-Sr/La bulks can be attributed to the presence of residual oxygen/nitrogen deficiencies. However, for the $SrTaO_2N$ bulk without additives, the anion vacancies are easily removed from the porous ceramic body to reach cation-anion stoichiometry. Accordingly, a more resistive bulk gave rise to a large semicircle in the impedance spectrum. For dielectric materials, low values of electrical resistance often lead to high dielectric loss; the increase in tan δ with the $SrCO_3$ or La_2O_3 additives could be related to the smaller bulk resistance.

In the present work, the dielectric permittivity of the dense $SrTaO_2N$ ceramics is extremely high and comparable with the giant ε_r reported for the rocksalt-type Li, Ti co-doped NiO [37]. In addition, the thermal stability of $SrTaO_2N$ can be ensured up to 480 °C in air [23], which is much higher than the Curie temperature of PZT [1], where a huge variation of permittivity occurs. Although the method of densification has been developed for the dielectric $SrTaO_2N$ ceramics, the dielectric loss should be further reduced by eliminating anion vacancies in a considerably improved microstructure.

Conclusion

Pressureless sintering was applied to fabricate dielectric oxynitride $SrTaO_2N$ ceramics using sintering additives. Both $SrCO_3$ and La_2O_3 were effective to achieve single-phase $SrTaO_2N$ bulks with relative densities higher than 90%. The incorporation of sintering additives in the $SrTaO_2N$ ceramic led to a well-developed microstructure with smaller grain sizes. The residual porosity of $SrTaO_2N$ ceramics was necessary to remove anion vacancies during the post-annealing treatment in ammonia to realize smaller dielectric losses. The room temperature ε_r values of $SrTaO_2N$-Sr and $SrTaO_2N$-La were 1.7×10^4 and 1.6×10^4 at 100 Hz, respectively; however, in contrast, the $SrTaO_2N$ without additives exhibited lower dielectric permittivity of approximately 1.8×10^3 due to the much higher porosity, the presence of secondary phases as well as the possible grain boundary effects.

Acknowledgement.

This work was partly supported by a Grant-in-Aid for Scientific Research on Priority Areas (Area #474, Gr #22015001) from the Ministry of Education, Culture, Sports, Science and Technology (MEXT) of Japan, and (A) (Gr #21245047) from the Japan Society for the Promotion of Science (JSPS). Y.-R. Zhang acknowledges financial support from the Global COE Program (Project No. B01: Catalysis as the Basis for Innovation in Materials Science) from MEXT.

Reference

1. Jaffe B, Cook Jr WR, Jaffe H. *Piezolelectric Ceramics*. London, New York: Academic Press Limited; 1971.
2. Cross LE. Relaxor ferroelectrics. *Ferroelectics* 1987;**76**:241-67.
3. Kim Y-I, Woodward PM, Baba-Kishi KZ, Tai CW. Characterization of the structural, optical, and dielectric properties of oxynitride perovskites AMO_2N (A = Ba, Sr, Ca; M = Ta, Nb). *Chem Mater* 2004;**16**:1267-76.
4. Kim Y-I, Si W, Woodward PM, Sutter E, Park S, Vogt T. Epitaxial thin-film deposition and dielectric properties of the perovskite oxynitride $BaTaO_2N$. *Chem Mater* 2007;**19**:618-23.
5. Ziani A, Le Paven-Thivet C, Le Gendre L, Fasquelle D, Carru JC, Tessier F, Pinel J. Structural and dielectric properties of oxynitride perovskite $LaTiO_xN_y$ thin films. *Thin Solid Films* 2008;**517**:544-9.
6. Lu Y, Ziani A, Le Paven-Thivet C, Benzerga R, Le Gendre L, Fasquelle D, Kassem H, Tessier F, Vigneras V, Carru J-C, Sharaiha A. Perovskite oxynitride $LaTiO_xN_y$ thin films: Dielectric characterization in low and high frequencies. *Thin Solid Films* in press.
7. Ebbinghaus SG, Abicht H-P, Dronskowski R, Müller T, Reller A, Weidenkaff A. Perovskite-related oxynitrides - Recent developments in synthesis, characterisation and investigations of physical properties. *Prog Solid State Chem* 2009;**37**:173-205.
8. Yang M, Oró-Solé J, Rodgers JA, Jorge AB, Fuertes A, Attfield JP. Anion order in perovskite oxynitrides. *Nat Chem* 2011;**3**:47-52.
9. Zhang Y-R, Motohashi T, Masubuchi Y, Kikkawa S. Local anionic ordering and anisotropic displacement in dielectric perovskite $SrTaO_2N$. *J Ceram Soc Jpn* 2011;**119**:581-6.
10. Bokov AA, Ye Z-G, Recent progress in relaxor ferroelectrics with perovskite structure, *J Mater Sci* 2006;**41**:31-52.
11. Banerjee A, Bandyopadhyay A, Bose S. Influence of La_2O_3, SrO, and ZnO addition on PZT. *J Am*

Ceram Soc 2006;**89**:1594-1600.

12. Malic B, Bernard J, Holc J, Jenko D, Kosec M. Alkaline-earth doping in (K,Na)NbO_3 based piezoceramics. *J Eur Ceram Soc* 2005;**25**:2707-11.
13. Fu P, Xu Z, Chu R, Li W, Zang G, Hao J. Piezoelectric, ferroelectric and dielectric properties of La_2O_3-doped $(Bi_{0.5}Na_{0.5})_{0.94}Ba_{0.06}TiO_3$ lead-free ceramics. *Mater Des* 2010;**31**:796-801.
14. Yang Y, Feng C, Yu Y. Low temperature sintering of PMN ceramics by doping with SrO. *Mater Lett* 2001;**49**:345-51.
15. Kim B-G, Cho SM, Kim T-Y, Jang HM. Giant dielectric permittivity observed in Pb-based perovskite ferroelectrics. *Phys Rev Lett* 2001;**86**:3404-6.
16. Yu Y, Tu J, Singh RN. Phase stability and ferroelectric properties of lead strontium zirconate titanate ceramics. *J Am Ceram Soc* 2001;**84**:333-40.
17. Rachel A, Ebbinghaus SG, Güngerich M, Klar PJ, Hanss J, Weidenkaff A, Reller A. Tantalum and niobium perovskite oxynitrides: Synthesis and analysis of the thermal behaviour. Thermochim Acta 2005;**438**:134-43.
18. Izumi F, Ikeda T. A Rietveld-analysis program RIETAN-98 and its applications to zeolites. *Mater Sci Forum* 2000;**321-4**:198-205.
19. Cole KS, Cole RH. Dispersion and absorption in dielectrics I. alternating current characteristics. *J Chem Phys* 1941;**9**:341-51.
20. Bednorz JG, Scheel HJ. Flame-fusion growth of $SrTiO_3$. *J Cryst Growth* 1977;**41**:5-12.
21. Zhang Y, Mack DE, Jarligo MO, Cao X, Vaβen R, Stöver D. Partial evaporation of strontium zirconate during atmospheric plasma spraying. *J Therm Spray Technol* 2009;**18**:694-701.
22. Pennec Y, Ingle NJC, Elfimov IS, Varene E, Maeno Y, Damascelli A, Barth JV. Cleaving-temperature dependence of layered-oxide surfaces. *Phys Rev Lett* 2008;**101**:216103.
23. Aguiar R, Logvinovich D, Weidenkaff A, Reller A, Ebbinghaus SG. Thermal oxidation of oxynitride perovskites in different atmospheres. *Thermochim. Acta* 2008;**471**:55-60.

24. Lu D, Hitoki G, Katou E, Kondo JN, Hara M, Domen K. Porous single-crystalline TaON and Ta_3N_5 particles. Chem Mater 2004;**16**:1603-5.

25. DiSalvo FJ, Clarke SJ. Ternary nitrides: a rapidly growing class of new materials. *Curr Opin Solid State Mater Sci* 1996;**1**:241-9.

26. Eck B, Dronskowski R, Takahashi M, Kikkawa S. Theoretical calculations on the structures, electronic and magnetic properties of binary 3d transition metal nitrides. *J Mater Chem* 1999;**9**:1527-37.

27. Toth LE. *Transition metal carbides and nitrides*. New York and London: Academic Press; 1971.

28. Shannon RD, Prewitt CT. Effective ionic radii in oxides and fluorides. *Acta Crystallogr* 1969;**B25**:925-46.

29. Chou X, Zhai J, Jiang H, Yao X. Dielectric properties and relaxor behavior of rare-earth (La, Sm, Eu, Dy, Y) substituted barium zirconium titanate ceramics. *J Appl Phys* 2007;**102**: 084106.

30. Zhou C, Liu X, Li W, Yuan C. Structure and piezoelectric properties of $Bi_{0.5}Na_{0.5}TiO_3$-$Bi_{0.5}K_{0.5}TiO_3$-$BiFeO_3$ lead-free piezoelectric ceramics. *Mater Chem Phys* 2009;**114**:832-6.

31. Kumar S, Varma KBR. Influence of lanthanum doping on the dielectric, ferroelectric and relaxor behaviour of barium bismuth titanate ceramics. *J Phys D: Appl Phys* 2009;**42**:075405.

32. Koval V, Alemany C, Briančin J, Bruncková H, Saksl K. Effect of PMN modification on structure and electrical response of *x*PMN-(1-*x*)PZT ceramic systems. *J Eur Ceram Soc* 2003;**23**:1157-66.

33. Zhang Y-R, Li J-F, Zhang B-P, Peng C-E. Piezoelectric and ferroelectric properties of Bi-compensated $(Bi_{1/2}Na_{1/2})TiO_3$-$(Bi_{1/2}K_{1/2})TiO_3$ lead-free piezoelectric ceramics. *J Appl Phys* 2008;**103**:074109.

34. Templeton A, Wang X, Penn SJ, Webb SJ, Cohen LF, Alford NM. Microwave dielectric loss of titanium oxide. *J Am Ceram Soc* 2000;**83**:95-100.

35. Negas T, Yeager G, Bell S, Coats N, Minis I. $BaTi_4O_9$/$BaTi_9O_{20}$-based ceramics resurrected for modern microwave applications. *Am Ceram Soc Bull* 1993;**72**:80-9.

36. Li M, Shen Z, Nygren M, Feteira A, Sinclair DC, West AR. Origin(s) of the apparent high permittivity in $CaCu_3Ti_4O_{12}$ ceramics: clarification on the contributions from internal barrier layer capacitor and sample-electrode contact effects. *J Appl Phys* 2009;**106**:104106.
37. Wu J, Nan C-W, Lin Y, D Y. Giant dielectric permittivity observed in Li and Ti doped NiO. *Phys Rev Lett* 2002;**89**:217601.

Figure Captions:

Fig. 1. XRD patterns of (a) as-nitrided $SrTaO_2N$ powder, (b) as-sintered $SrTaO_2N$ bulk, (c) as-sintered $SrTaO_2N$-Sr bulk, (d) as sintered $SrTaO_2N$-La bulk, (e) post-annealed $SrTaO_2N$ bulk, (f) post-annealed $SrTaO_2N$-Sr bulk, and (g) post-annealed $SrTaO_2N$-La bulk.

Fig. 2. Scanning electron micrographs of the fracture surfaces of post-annealed (a) $SrTaO_2N$ without additives, (b) $SrTaO_2N$-Sr, and (c) $SrTaO_2N$-La bulks.

Fig. 3. Relative dielectric constants (ε_r) and dielectric losses ($\tan \delta$) of post-annealed (a) $SrTaO_2N$ without additives, (b) $SrTaO_2N$-Sr, and (c) $SrTaO_2N$-La bulks as a function of frequency.

Fig. 4. Impedance spectra for the post-annealed $SrTaO_2N$ ceramics measured at 10^2-10^6 Hz.

Table 1.

Summary of structural refinement details for the as-nitrided $SrTaO_2N$ powder, as-sintered and post-annealed $SrTaO_2N$ products.

	As-nitrided	As-sintered	Post-annealed
Crystal system		Tetragonal	
Space group		*I*4/*mcm*	
a (nm)	0.5700(3)	0.5701(3)	0.5701(5)
c (nm)	0.8078(2)	0.8068(4)	0.8076(4)
$c/\sqrt{2}a$	1.0021	1.0006	1.0017
Volume ($10^{-27}m^3$)	0.2625(4)	0.2622(2)	0.2625(3)
ρ_{calc} ($Mg \cdot m^{-3}$)	7.9607(3)	7.9680(5)	7.9613(2)
$SrTaO_2N$ (wt%)	99.57	97.68	98.13
TaC (wt%)	--	2.32	0.89
Ta_3N_5 (wt%)	--	--	0.98
R_{wp} (%)	7.13	9.32	9.37
S	1.94	2.48	2.49

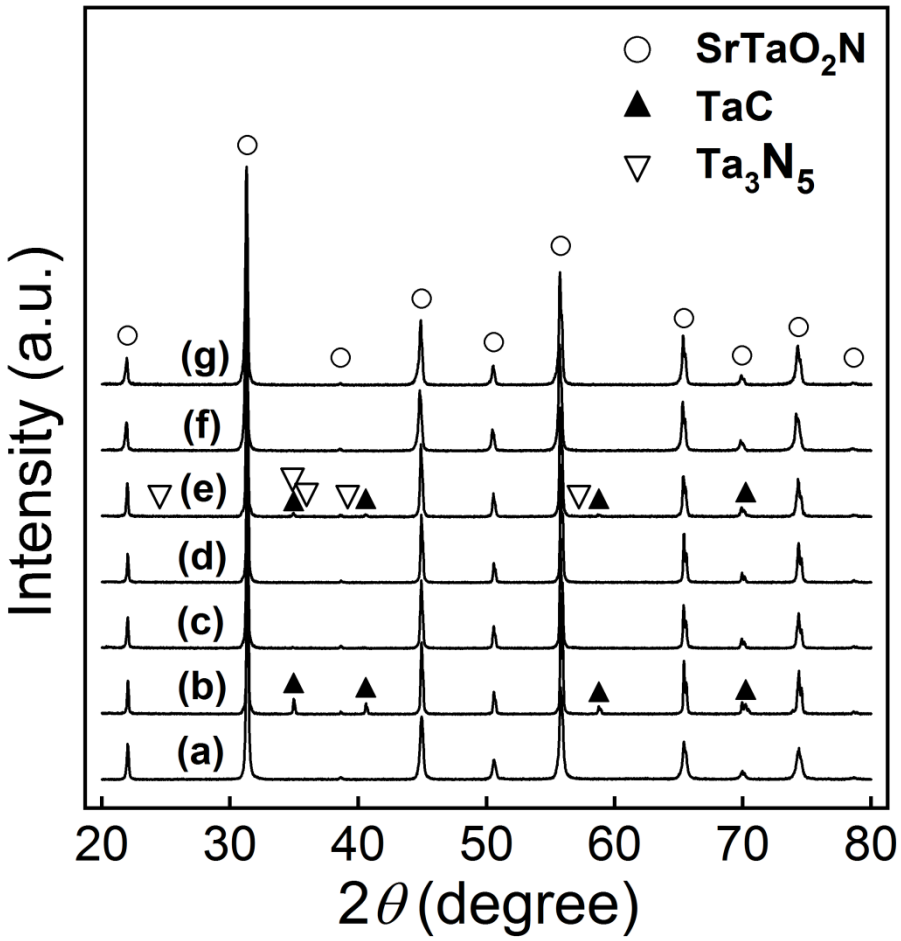

Fig. 1. XRD patterns for (a) as-nitrided $SrTaO_2N$ powder, (b) as-sintered $SrTaO_2N$ bulk, (c) as-sintered $SrTaO_2N$-Sr bulk, (d) as sintered $SrTaO_2N$-La bulk, (e) post-annealed $SrTaO_2N$ bulk, (f) post-annealed $SrTaO_2N$-Sr bulk, and (g) post-annealed $SrTaO_2N$-La bulk.

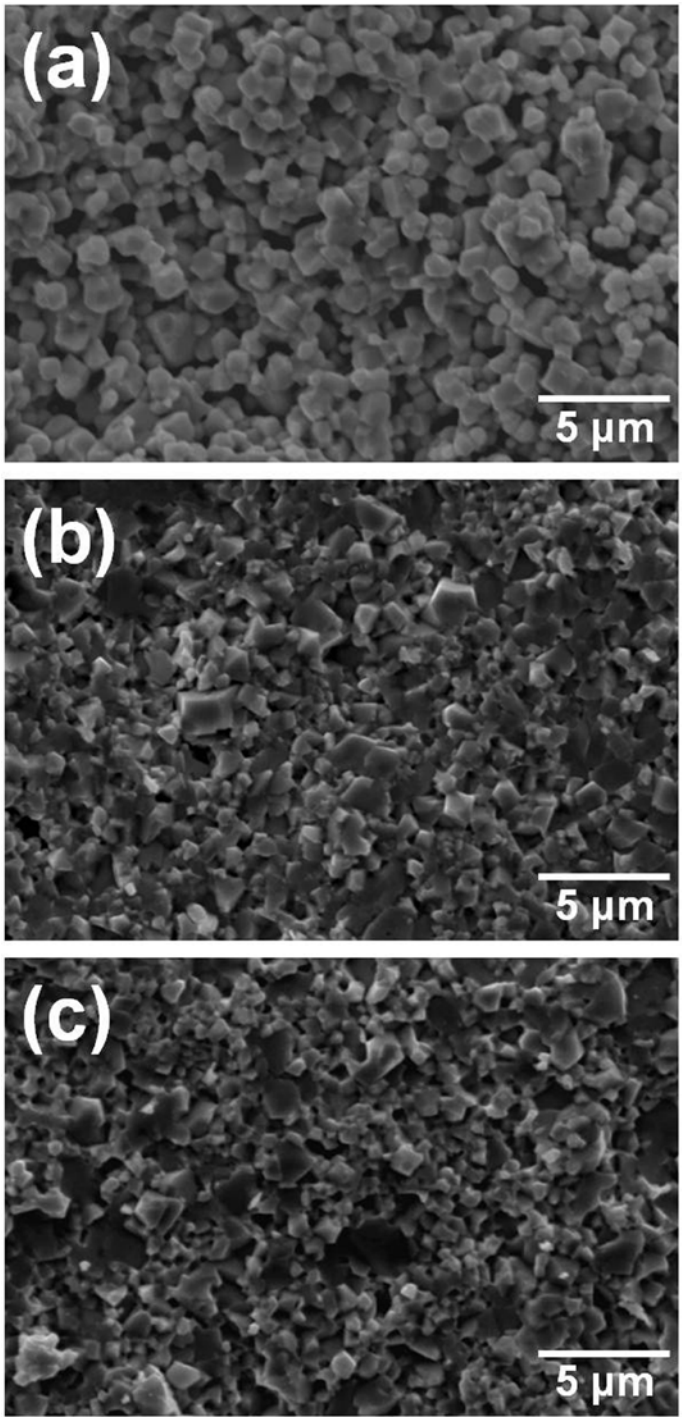

Fig. 2. Scanning electron micrographs of the fracture surfaces of post-annealed (a) $SrTaO_2N$ without additives, (b) $SrTaO_2N$-Sr, and (c) $SrTaO_2N$-La bulks.

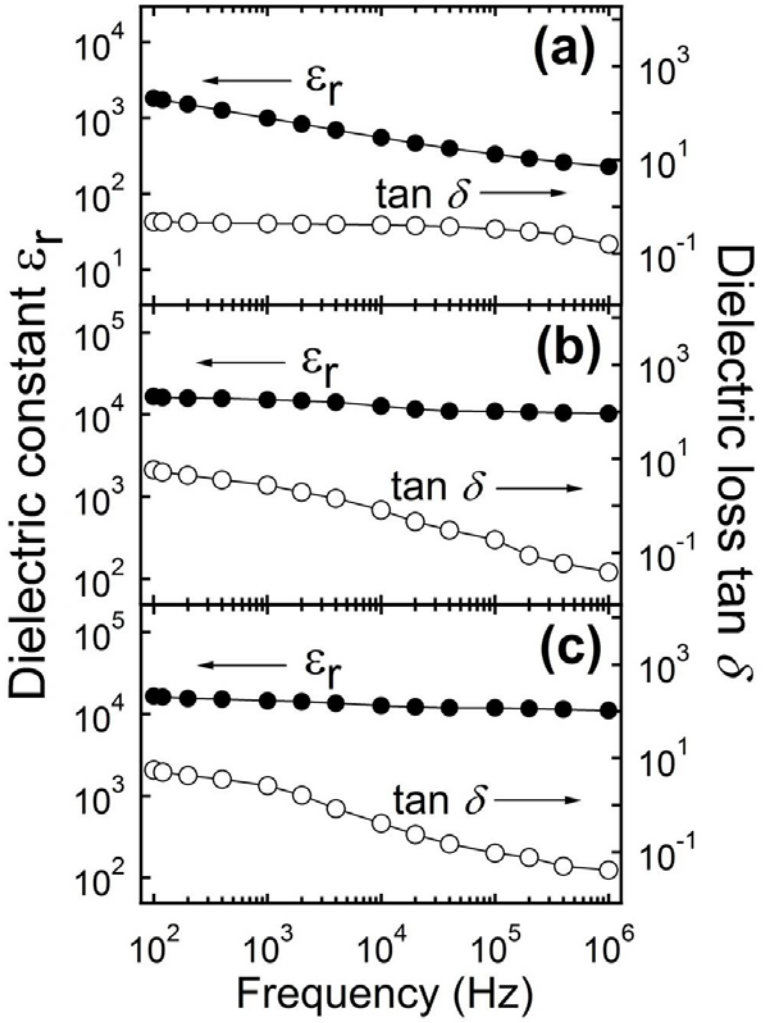

Fig. 3. Relative dielectric constants (ε_r) and dielectric losses (tan δ) of post-annealed (a) $SrTaO_2N$ without additives, (b) $SrTaO_2N$-Sr, and (c) $SrTaO_2N$-La bulks as a function of frequency.

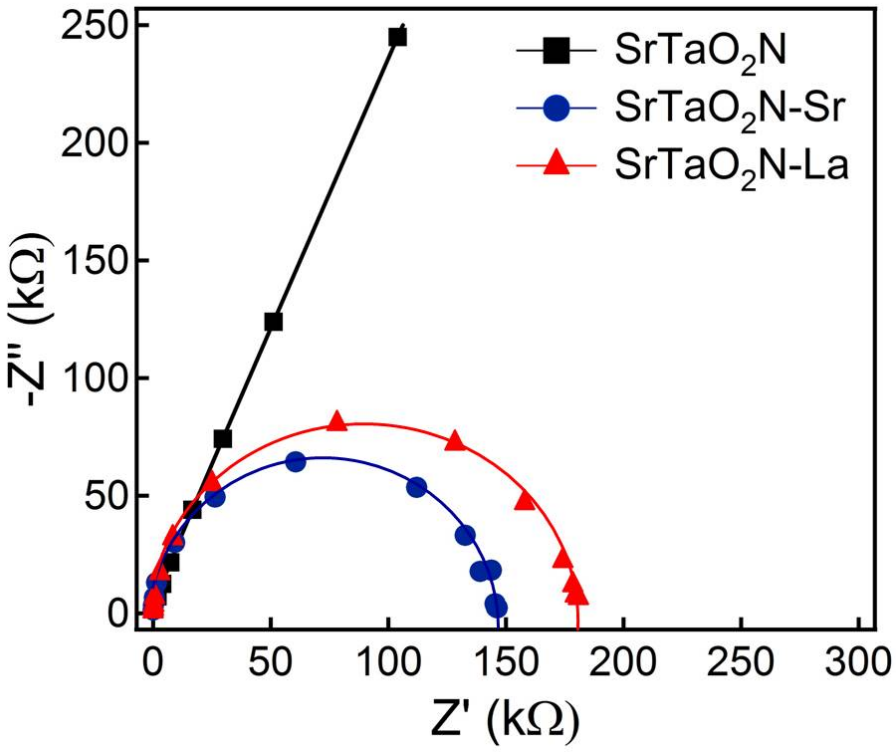

Fig. 4. Impedance spectra for the post-annealed $SrTaO_2N$ ceramics measured at 10^2-10^6 Hz.